Biointerphases
a SpringerOpen Journal

PERSPECTIVE Open Access

A virus biosensor with single virus-particle sensitivity based on fluorescent vesicle labels and equilibrium fluctuation analysis

Marta Bally[1*], Moritz Graule[1], Francisco Parra[2], Göran Larson[3] and Fredrik Höök[1*]

Abstract

Biosensors allowing for the rapid and sensitive detection of viral pathogens in environmental or clinical samples are urgently needed to prevent disease outbreaks and spreading. We present a bioanalytical assay for the detection of whole viral particles with single virus sensitivity. Specifically, we focus on the detection of human norovirus, a highly infectious virus causing gastroenteritis. In our assay configuration, virus-like particles are captured onto a supported lipid bilayer containing a virus-specific glycolipid and detected after recognition by a glycolipid-containing fluorescent vesicle. Read-out is performed after illumination of the vesicle labels by total internal reflection fluorescence microscopy. This allows for visualization of individual vesicles and for recording of their binding kinetics under equilibrium conditions (equilibrium fluctuation analysis), as demonstrated previously. In this work we extend the concept and demonstrate that this simple assay setup can be used as a bioanalytical assay for the detection of virus particles at a limit of detection of 16 fM. Furthermore, we demonstrate how the analysis of the single vesicle-virus-like particle interaction dynamics can contribute to increase the accuracy and sensitivity of the assay by discriminating specific from non-specific binding events. This method is suggested to be generally applicable, provided that these events display different interaction kinetics.

Keywords: Virus detection, Biosensor, Norovirus, Glycosphingolipids, Phospholipid vesicle, Nanoscale label, Fluorescence, Liposome, Virus-like particle

Background

Over the last decades, increasing effort has been put into the development of bioanalytical devices allowing for the detection of biological compounds in environmental or human samples. Such biosensors commonly take advantage of specific binding between a molecule of interest (target) and a biological counterpart (e.g. receptor-ligand, antigen-antibody or complementary oligonucleotides) to detect the presence of the target with high specificity. Generally speaking, one can distinguish between solution-based assays usually combined with beads or nanoparticles, and heterogeneous surface-based assays [1-3]. In the latter case, a variety of biosensors relying on the generation of *e.g.* optical, electrical or gravimetric signals has been described, of which optical detection in conjunction with biomolecule labeling is nowadays the most widespread [4,5]. In this approach, a detectable fluorescent, colorimetric or chemiluminescent signal is generated by a label attached to a reporter biomolecule that binds specifically to the target, which is in turn bound to the sensor surface via a capture probe (e.g. receptor, antibody, oligonucleotide. . .) [6,7].

In the context of environmental monitoring and medical diagnostics, biosensors for the detection of viral pathogens have recently attracted considerable interest: rapid identification of the presence of a virus in *e.g.* contaminated food or water or in a patient's sample is a prerequisite to efficiently counteract viral outbreaks, epidemics or bioterrorism. Today, the highest sensitivity for virus detection is achieved with assays relying on polymerase chain reaction (PCR) for multiplication and detection of viral DNA and RNA [8]. Major drawbacks of this technique are however the long processing time (typically 24 hours), the need for advanced laboratory equipment and trained personnel, as

* Correspondence: bally@chalmers.se; fredrik.hook@chalmers.se
[1]Department of Applied Physics, Division of Biological Physics, Chalmers University of Technology, Göteborg SE-412 96, Sweden
Full list of author information is available at the end of the article

well as lack of real-time monitoring and rapid on-site pathogen detection. This calls for the development of simple field-oriented devices capable of detecting the pathogen with high sensitivity and accuracy. In particular, efforts have been directed at the implementation of assays allowing for the detection of whole viral particles in a variety of sensor formats. Optical detection often relies on virus capture and detection in a sandwich assay format in which a molecule immobilized on the sensor surface, captures the target analyte (e.g. a viral particle). A detectable signal is then generated after subsequent binding of a reporter molecule carrying a suitable label. Read-out has been performed with a variety of methods, including fluorescence [9-11], enzyme-linked immunosorbent assays [8,12] and using gold colloids for visual [13] or Surface Enhanced Raman Scattering (SERS) [14] detection. In view of their potential for miniaturization and their relatively simple read-out schemes, optical sandwich assays have been combined to dipstick-like sensors (lateral flow assays) [13] or microfluidic setups which make it possible to engineer assays exhibiting a reduced sample consumption or including a sample enrichment step [9,10]. Together with detection limits in the 10–100 fM (10^6–10^7 particles/ml) range [9], this makes such sensors promising candidates for field-oriented applications. As an alternative to such optical sandwich-based assays, approaches proposed in the context of viral particle detection rely, for example, on direct label-free optical detection [15], on the use of functionalized microcantilevers [16], on the detection of virus-induced assembly of magnetic nanoparticles [17] or on electrical [18] and electrochemical [19] transduction.

The growing need for biosensors combining high sensitivity and short processing time, as required *e.g.* for the detection of virus particles in environmental samples, has also stimulated the development of assays with single-molecule sensitivity, *i.e.* assays capable of detecting the signal generated by individual target-bound reporter molecules at a sensing interface. In such assays, the targets can be individually counted and the limit of detection (LOD) of the biosensor is not limited by the sensitivity of the transducer, but rather by other limiting factors connected with the bioanalytical assay itself. A relatively simple approach to reach single-molecule sensitivity relies on the use of micro- or nanoscale labels generating a strong signal (via e.g. scattering or fluorescence). Instead of depending on the transducer sensitivity, the LOD is, in this case, rather related to non-specific binding events, leading to an increased background signal, but also to the affinity between the ligand and the receptor, which determines the surface coverage, as well as the target incubation time, which depends on diffusion limitations. A variety of biosensors making use of metallic or semi-conductor nanoparticles [13,14,20], polymeric microparticles [21], or lipid vesicles [9,22,23] for signal amplification has been developed [7], of which a few specifically take direct advantage of the individual visualization of the particles for read-out [21,22,24-27].

In the context of nanoscale labels for biosensing applications, phospholipid vesicles – hollow water-filled shells self-assembled from lipids – are particularly interesting candidates: functional biomolecules such as proteins or glycolipids, but also fluorescent markers, can be easily incorporated into the bilayer membrane or attached to it. In addition, either their interior or the lipid bilayer membrane itself can contain reporter molecules for signal generation [7]. Importantly, phosphocholine-containing bilayers are also known to exhibit excellent anti-fouling properties, resulting in low non-specific adsorption of proteins [28]. Moreover, vesicles represent minimal cell membrane models making them well-suited for studies of biomolecular reactions occurring at the cell membrane surface [23,29,30].

Our group has recently presented a method to probe the interaction between a surface-immobilized target and functional fluorescent vesicles using total internal reflection fluorescence (TIRF) microscopy [26,31-34]. The method takes advantage of the surface confinement of the evanescent field of TIRF to visualize individual sensor-bound vesicles while filtering out the fluorescence background generated from out-of-focus vesicles. Beyond the use of vesicles as signal enhancing elements to reach single-molecule sensitivity, real-time monitoring of vesicle binding and release events under equilibrium binding conditions (equilibrium fluctuation analysis) makes it possible to extract quantitative information on the biomolecular reaction under investigation: recording of the number of newly arrived vesicles over time can be related to the association behavior and used to quantify the association rate constant [32]. In addition, simultaneous analysis of the residence time of the vesicles is related to the dissociation behavior and can yield information on the dissociation rate constant [33]. In particular, this method makes it possible to probe both weak (> μM) and strong (< pM) interactions, because binding events are visualized individually. For example, equilibrium fluctuation analysis has been used to probe and quantify the interaction kinetics between a ligand and cell-membrane bound receptors [33] (K_D in the low nM range), weak glycosphingolipid-glycoshingolipid (GSL) interaction (Kunze *et al.* Equilibrium fluctuation analysis of single liposome binding events reveals how cholesterol and Ca^{2+} modulate glycosphingolipid trans-interactions, submitted) (K_D in the low mM range) as well as the interaction between virus-like particles (VLP) from the norovirus and GSL- containing membranes [31,32].

The equilibrium fluctuation analysis method has so far primarily been used to extract kinetic and thermodynamic information, while its capacity to detect low amounts of

target molecules has so far only been explored for DNA detection [26]. The reported fM detection limit suggests that the concept represents a promising alternative, also in the development of viral biosensors. Moreover, the possibility of discriminating interactions according to their kinetic behavior opens the possibility of developing alternative means to determine whether an interaction is of specific or non-specific type. This novel aspect of the concept was, in this work, explored for the detection of human norovirus (NoV). VLPs of the Ast/6139/01 strain from the most common norovirus II.4 genogroup were used as models for the pathogen. NoV is a small non-enveloped RNA virus of the Caliciviridae family with a high genetic diversity. It consists of an outer icosahedral shell assembled mainly from 180 capsid proteins (56 kDa) which protect the viral genome [35]. The acute gastroenteritis caused by the NoV, also called "winter vomiting disease", is globally spread through pandemics, and is recognized to be responsible for over 200.000 yearly deaths mainly in children in developing countries. In other countries mainly institutionalized, elderly and immunosuppressed patients are specifically at risk, and the harm caused during outbreaks should not be underestimated. This enteric virus spreads globally mostly through the oral-fecal route and spontaneous outbreaks often occur after consumption of contaminated food or water. NoVs are environmentally very stable and extremely infectious which makes their surveillance *e.g.* in water supplies highly demanding: only very low particle numbers (<100) might be sufficient to generate disease outbreaks making its early detection particularly challenging [36]. In lack of *in vitro* culture systems, self-assembled capsid proteins recombinantly expressed in insect cells are often used to probe the binding behavior of the virus. These non-infectious VLPs exhibit a morphology and binding properties similar to those of real viruses [37] and are known to recognize with high specificity a variety of saliva and cell-surface glycoconjugates, including membrane bound histo-blood group active GSLs [38]. Such VLPs thus represent excellent models in work aimed at designing new biosensor principles for virus detection.

The assay explored in this work is based on a sandwich-type configuration where the VLPs are first captured onto a non-fouling supported lipid bilayer containing a NoV-specific GSL ligand. The firmly bound NoVs are then visualized by imaging individual fluorescently-labeled phospholipid vesicles containing the same NoV-specific ligand. A considerable amount of vesicles was found to interact reversibly with the VLPs, which is attributed to a vesicle-curvature dependent interaction strength [32]. This allows for real-time recording of binding kinetics under equilibrium conditions. We further make an attempt to take advantage of the vesicle association and dissociation dynamics to improve the accuracy and LOD of the assay, by discriminating specific and non-specific binding events according to their kinetic signatures.

Methods

Materials

1-Palmityol-2-Oleyol-sn-Glycero-3-Phosphocholine (POPC) was purchased from Avanti Polar Lipids (USA) while 1% Lissamine-Rhodamine B-1,2-dihexadecanoyl-sn-glycero-3-phosphatidylethanolamine (rhodamine-DHPE) was obtained from Invitrogen (USA). Histo-blood group H type 1 GSL [38,39] was purified from human meconia, pooled according to the ABO blood group and characterized by mass spectrometry and ^{1}H-NMR spectroscopy [40,41]. VLPs from the Spanish norovirus isolate Ast6139/01/Sp [42] (accession number: CAE47529) were produced as described previously [43]. The VLP concentration was determined from the total protein content using a molecular weight of $1.17*10^{4}$ kDa (the VLP consists of 180 copies of a 56 kDa recombinant capsid protein). This value was in good agreement with the number of particles counted by nanoparticle tracking analysis (performed with Nanosight LM 120 instrument placed on an optical microscope at 20X magnification). All experiments were performed in filtered TRIS buffer (10 mM Tris(hydroxymethyl)-aminomethane, 100 mM NaCl, pH 7).

Lipid vesicle preparation

Lipid vesicles were prepared by the lipid film hydration and extrusion method. Briefly, POPC, H type 1 GSL, and if needed, rhodamine-DHPE lipids diluted in chlorophorm were mixed in appropriate amounts and dried first under a gentle nitrogen stream and then under vacuum for at least 1.5hours. The lipid film was then hydrated in TRIS buffer while vortexing. The so-obtained vesicle suspension was extruded by pushing the suspension a defined number of times through polycarbonate membranes (pore size: 30 nm or 100 nm). The vesicles were stored at 4°C until use.

Assay preparation

All experiments were performed in glass-bottom microtiter wells (96 well-plate) that were cleaned overnight in a 10 mM sodium dodecyl sulfate solution and rinsed thoroughly with MilliQ water. Supported lipid bilayers were formed at the bottom of the microwells by surface-induced vesicle fusion [44]. For this purpose, vesicles containing 10% H type 1 GSL (extruded 11 times at 30 nm) were added to the well (total lipid concentration 0.1 mg/ml). After incubation for 30 min, the total volume of the well was adjusted with buffer to 100 μl and rinsed carefully 8 times with 200 μl of buffer without drying the surface. After rinsing, 50 μl of VLP suspension were added (total volume in the well: 100 μl) and incubated for 1 hour. This was followed by rinsing and addition of POPC vesicles (final concentration: 0.05 mg/ml, extruded 21 times at

100 nm). After at least 10 min, fluorescent vesicles containing 5% H type 1 GSL and 3% rhodamine-DHPE (extruded 21 times, 100 nm) were added, yielding a final concentration of 0.25 μg/ml. Read-out was performed at least 30 min after addition of the fluorescent vesicles to make sure that equilibrium conditions were reached.

Data acquisition

Time-lapse movies were acquired on a Nikon Eclipse Ti-E inverted microscope using a 60X magnification (NA = 1.49) oil immersion objective (Nikon Corporation, Japan). The microscope was equipped with a mercury lamp (Intensilight C-HGFIE; Nikon Corporation), a TRITC filter cube (Nikon Corporation) and an Andor iXon + EMCCD camera (Andor Technology, Northern Ireland). Movies consisting of 1000 frames were taken at an acquisition rate of 5 frames/second. For each well, 7 different positions were imaged to ensure good statistics, as bilayer quality and VLP surface coverage may vary within one well.

Data-analysis

Images were processed and analyzed with MatLab (MathWorks, Inc., USA) based on a method described in detail elsewhere [26]. Briefly, a fluorescent vesicle was counted if its intensity exceeded a pre-set threshold and if it was present on a pre-defined number of consecutive frames (minimum 7 frames). Association plots were generated by recording the number of newly arrived vesicles (n_+) over time. The program further analyses the residence time ($\Delta\tau$) of these vesicles. To ensure accurate statistics of the residence time analysis, only the vesicles that arrived in the first half of the movie were considered and the maximal residence time was set to half of the total measurement time. Moreover, bleached vesicles, which disappeared without exhibiting a sudden drop in intensity, were discarded from the analysis. Residence time analysis was used to reconstruct the dissociations plots which display the number of vesicles that are still bound as a function of time.

Movies of insufficient quality (due e.g. to the apparition of aggregates in the field of view) were discarded automatically by the software. To decide whether a movie should be taken into account for evaluation, the slope of the association signal was compared to the average signal of the other movies for the same sample. If this value differed more than two standard deviations (of the signal of the remaining movies) from the average signal, this movie was discarded. A minimum of 3 movies was used for the evaluation.

To generate association plots and for the residence time analysis, as well as to estimate the surface coverage, the data obtained from all movies taken within the same microwell (3–7 movies/well) was summed up and normalized to the total area imaged. To make up for inconsistencies in the final volume associated with the numerous pipetting steps, all signals were normalized by multiplying with the final well content (determined by weighting). The average image intensity was measured with Image J (Image processing and analysis in Java, National Institute of Health, USA); each data point was the average of all the frames taken within a well. To determine the equilibrium surface coverage (n_{eq}), only the vesicles bound for more than 50 frames (10 s) were counted. The slope of association ($\delta n_+ / \delta t$) was determined by fitting the data with a linear fit $y = a^*x$. The area under the dissociation curve (A_{diss}) was determined after fitting the data with a double exponential function $y = a^*\exp(bx) + c^*\exp(dx)$.

Evaluation of the limit of detection

To determine the LOD of the assay a 4-fold VLP dilution series was prepared. At least 8 VLP concentrations were included in each experiment and added to a microwell which was imaged at 7 different locations. The VLP concentration in the wells ranged from 125 ng/ml (12.5 pM) to 0.122 ng/ml (12.1 fM). The signal for a well where no VLPs were added was used as a negative control. The LOD was determined from the mean signal of the negative control incremented with the 3-fold standard deviation of three independent experiments. In this case, the procedure mentioned above was reproduced independently on different days using freshly prepared VLP dilutions.

Results

The assay designed for the fluorescence-based detection of unlabeled NoV VLPs using TIRF microscopy utilizes a microwell functionalized with a POPC supported lipid bilayer containing 10% H type 1 GSL. POPC bilayer coatings have been shown to render glass surfaces highly resistant against non-specific protein and vesicle binding [28] while the GSLs ensure a high capture efficiency and specificity to the NoV VLPs [32,39]. Fluorescently labeled vesicles containing H type 1 GSL for specific recognition were used to detect firmly bound VLPs by TIRF microscopy (Figure 1a). The vesicles contained a large amount of fluorophores (~3000 fluorophores / vesicle). This enables the visualization of each vesicle individually (Figure 1b), and confers the single VLP sensitivity of the method. As visible in Figure 1b, the sensor exhibited a good specificity with little non-specific binding on the negative controls performed in the absence of VLPs.

Taking advantage of the evanescent field generated by the TIRF illumination to discriminate surface-bound vesicles from the ones in solution, vesicle binding and release events at the sensor interface were recorded under steady-state, *i.e.* equilibrium binding conditions.

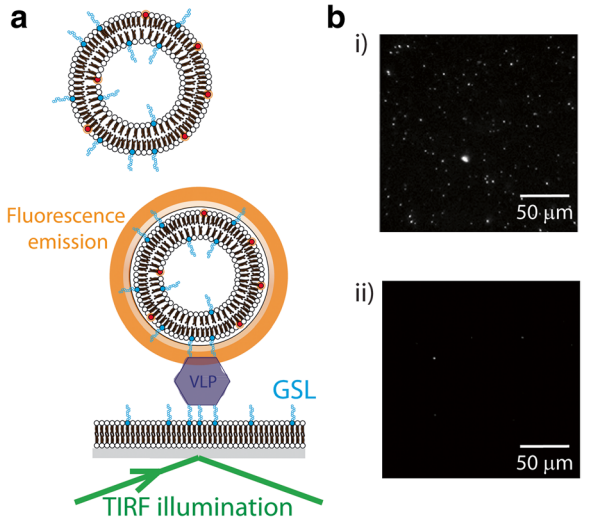

Figure 1 a) Detection of norovirus virus-like particles (VLP) by total internal reflection fluorescence (TIRF). a) Schematic representation of the sandwich assay setup. The particles are captured onto a bilayer containing 10% H type 1 glycosphingolipids (GSL) recognizing the VLPs with high specificity. The fluorescent signal is generated by TIRF illumination of the sensor-bound rhodamine-labeled vesicles containing 5% H type 1 GSL. **b**) A representative microscopy image of surface-bound vesicles i) on a bilayer incubated with 12.5 pM VLPs and ii) on a negative control performed in absence of VLPs. Scale bars: 50 µm.

The equilibrium coverage (n_{eq}), the rate of arrival of new vesicles at steady state ($\delta n_+/\delta t$) and the residence times ($\Delta\tau$) of the individual vesicles were extracted after analysis of the time-lapse movies and used to quantify the sensor signal. All results presented were recorded at least 30 min after adding the vesicles to make sure that the system had enough time to relax towards equilibrium. In these conditions, the average number of vesicles bound to the substrate did not vary over time (Figure 2a) while the number of newly arrived vesicles increased linearly (Figure 2b). Both observations confirm that the measurement is indeed performed under steady-state conditions.

The distribution of the residence time of the vesicles (Figure 2c) can be converted into dissociation plots displaying the number of vesicles still bound over time (Figure 2d). The latter curves reveal that over the duration of the measurement ($\Delta\tau$ is analyzed for 100 s) a major fraction of vesicles was released (~ 80%, for the case shown in Figure 2d) while the remaining fraction was considered as irreversibly bound on the time scale of the measurement. At this VLP concentration (12.5 pM), the positive signal was clearly distinguishable from the negative background signal (experiment performed in absence of VLPs), further illustrating the sensor specificity (red vs. blue curves in Figure 2). Note in particular, that in Figure 2c most of the non-specific reversible events had $\Delta\tau$ < 10 s (blue curve) while for the specific signal (red curve) a significant number of events had a residence time 10 s < $\Delta\tau$ < 100 s, indicating that a discrimination of both types of interactions according to their kinetic signature could be possible.

In analogy to conventional end-point measurements, the sensor signal can be evaluated by counting the individual surface-bound vesicles under equilibrium conditions and using n_{eq} as a measure for the sensor signal. A typical response curve, displayed as signal-to-background (s/b) vs. concentration for a sample dataset, is shown in Figure 3a (green squares). Here, the number of bound vesicles counted (n_{eq}) obtained for positive (in the presence of VLPs) and negative (in the absence of VLPs) samples are taken as the signal and the background, respectively. As an alternative to n_{eq}, the signal can be evaluated by measuring the average frame intensity (I_{frame}), in analogy to fluorescence-based assays lacking single-molecule sensitivity. As shown in Figure 3a (light blue dots) no contrast was observed at any concentration, illustrating the advantage of an evaluation based on individual label counts.

We also specifically investigated whether real-time equilibrium fluctuation analysis of the recognition reaction can further contribute to increase the accuracy of the assay. The vesicle arrival rate ($\delta n_+/\delta t$) is expected to correlate with the VLP surface concentration [32]. For analysis, $\delta n_+/\delta t$ was therefore used as a measure for the sensor signal and obtained by linear fit of the association curve (Figure 2b). To optimize the s/b, we investigated whether it is possible to take advantage of the differences in the kinetic signatures of specific and non-specific interactions (see e.g. Figure 2c) to further reduce the background, thus increasing the s/b ratio. A close look at the $\Delta\tau$ distribution for both cases (Figure 2c) reveals that, in absence of VLPs, the vesicles interact weakly with the supported lipid bilayer, and that most of them have residence times of less than 10 seconds ($\Delta\tau$<10 s). To illustrate how an appropriate data analysis strategy can be used to maximize s/b values and hence to increase the sensor's accuracy, we have compared different evaluation strategies using a representative dataset. For this dataset, the $\delta n_+/\delta t$ was evaluated by considering only the vesicles that had $\Delta\tau$ > 10s (Figure 3b red diamonds). Here, this evaluation strategy yields a ~3.5-fold increase in s/b compared to the case where all vesicles are taken into account and an increase by a factor ~2 compared to an evaluation of the vesicle equilibrium surface coverage (n_{eq}).

In this context, it should be mentioned that the quality of the bilayer and its non-fouling properties can depend on the overall quality of the substrate. For bilayers of outstanding quality, less than 10% of the vesicles were irreversibly bound. However, an increase in the number of vesicles irreversibly attached to the bilayer was observed occasionally, most likely originating from non-specific binding due to the presence of defects in the coating. In such a case, the

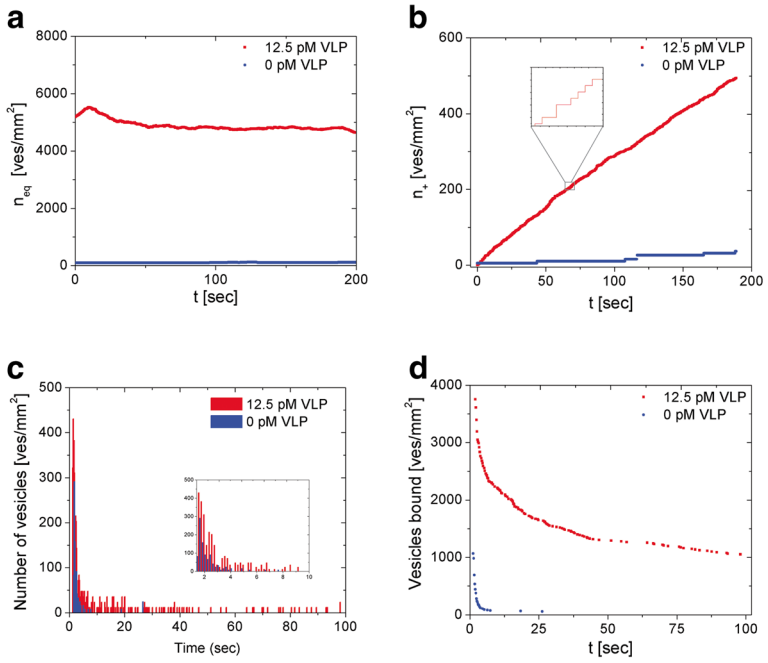

Figure 2 Equilibrium fluctuation analysis of vesicle – virus-like particle (VLP) interactions. a) Equilibrium surface coverage (n_{eq}) vs. time. **b**) number of newly arrived vesicles (n_+) vs. time. The insert illustrates that individual binding events are recorded. **c**) Residence time ($\Delta\tau$) distribution of the newly arrived vesicles. **d**) Dissociation plot displaying the number of vesicles still bound vs. time. In all cases a positive signal recorded on a substrate incubated with 12.5 pM VLPs (red) is compared to a negative control performed in absence of the VLPs (blue).

percentage of irreversible events could be as high as 70% of the total events (see Additional file 1: Figure S1). An additional data analysis was therefore performed by further discarding the irreversibly bound vesicles from the analysis, and taking therefore into consideration only the events that had a residence time of 10 s < $\Delta\tau$ < 100 s. For the data set presented in Figure 3, which had an irreversible fraction of 39% (see Additional file 1: Figure S1), this analysis yields an increase in s/b by a factor 3.5 (Figure 3b, blue stars) compared to the evaluation performed with $\Delta\tau$> 10 s (Figure 3b red diamonds).

We thus conclude that for an analysis based on the use of $\delta n_+ / \delta t$ as the signal, the highest s/b is obtained by analyzing the data for 10 s < $\Delta\tau$ < 100 s as the non-specific interactions appear to be predominantly either very transient ($\Delta\tau$ < 10 s) or irreversible (> 100 s).

An alternative evaluation strategy makes use of the contrasts in the dissociation curves (Figure 2d) to determine

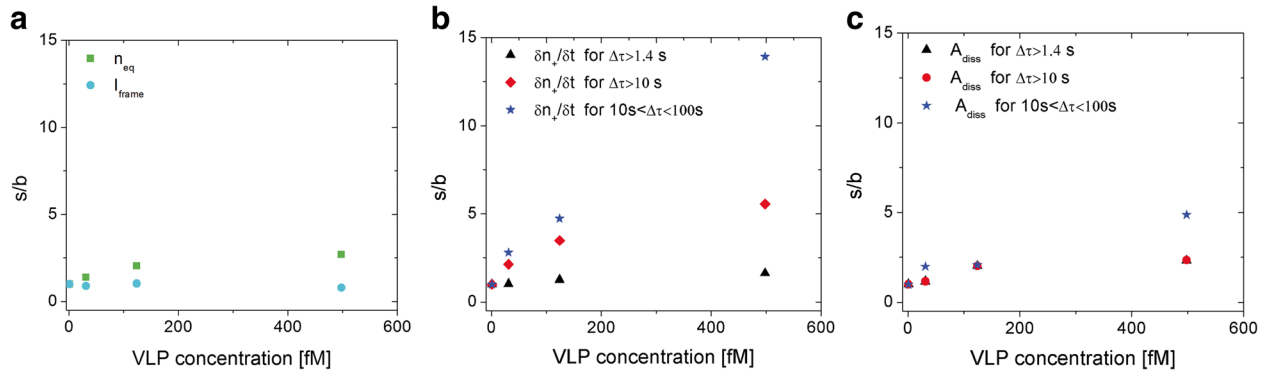

Figure 3 Response curves displaying the signal-to-background (s/b) vs. concentration for a chosen data set analyzed with different strategies. **a**) After evaluation of the surface-bound vesicles at equilibrium. Evaluation was performed either by vesicle counting (green squares) or by measuring the average image intensity (light blue dots). **b**) Using the vesicle arrival rate ($\delta n_+ / \delta t$) as a signal. **c**) Using the area under the dissociation curve (A_{diss}). Evaluation was performed taking all events into account (black triangles), for $\Delta\tau$ > 10 s, *i.e.* after removing of all events with a short residence time (red dots) or for 10 s < $\Delta\tau$ <100 s, *i.e.* after removing the events with a short residence time and the irreversibly bound vesicles (blue stars). In all cases, the background signal was the signal measured on the negative control.

the sensor signal. In this case, the area under the curve (A_{diss}) is measured after fitting the dissociation with a suitable analytical function, here a double exponential function. In analogy to the analysis performed above, all vesicles were taken into account ($\Delta\tau$ > 1.4 s, Figure 3c black triangles) or the vesicles were selected in order to discriminate specific and non-specific interaction ($\Delta\tau$ > 10 s, Figure 3c red dots; or 10 s < $\Delta\tau$ <100 s Figure 3c, blue stars). Generally, the s/b values obtained this way were lower than for the evaluation obtained using $\delta n_+ / \delta t$ and the data were of inferior quality.

The LOD of the bioanalytical assay for the detection of NoV VLPs was determined from three independent measurements with irreversible fractions on the negative controls of 5.5%, 5.5% and 2% respectively. Based on the analysis above, all reversible events above 10 s (10 s < $\Delta\tau$ < 100 s) were taken into consideration, and $\delta n_+ / \delta t$ was used as signal. For all three experiments the non-specific binding events were successfully filtered out and the background signal was indeed zero. In this case, the lowest detected signal was 12.1 fM, indicating that the assay sensitivity is in the low fM range (Figure 4). The signal depended linearly on the VLP concentration for a concentration range spanning over at least 3 orders of magnitude. Since for these experiments, the irreversibly bound fraction on the negative controls was low and therefore not expected to significantly influence the assay sensitivity, we further analyzed the data with $\Delta\tau$ > 10 s to provide a quantitative estimation of the LOD while taking the measurements standard deviations into account. This yields a detectable background signal (see Additional file 1: Figure S2 for the response curve) and the assay LOD estimated from the background signal incremented with its 3-fold standard deviation was 15.8 fM.

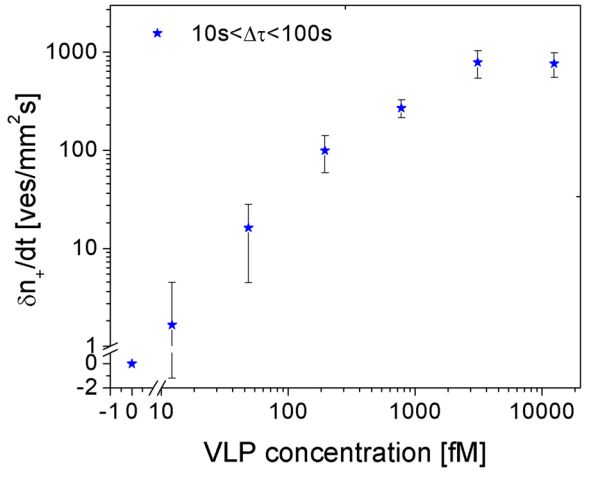

Figure 4 Response curve displaying the signal vs. virus-like particle (VLP) concentration. The signal is the slope of association curve (rate of arrival of new vesicles, $\delta n_+ / \delta t$) using a residence time interval 10 s < $\Delta\tau$<100 s. Each data point is the average of three independent measurements (2 for the 12.5 pM data point). The error bars are the standard deviation of three independent experiments.

Discussion

We have presented a biosensor for the fluorescence-based detection of NoV VLPs using TIRF illumination and fluorescently labeled vesicles to generate an optical contrast upon recognition of the VLP. The method exhibits single-molecule sensitivity, as individual vesicles can be readily visualized.

As compared to conventional fluorescence read-out based on average fluorescence intensity measurements of the sensing area, the possibility of imaging individual fluorescent reporter biomolecules – the vesicles in this case - and counting them one by one, represents a simple approach to increase the s/b ratio of a sensor, and hence to increase the reliability while maximizing the sensitivity. This is due to the fact that the vesicles generate localized signals which can be easily resolved and discriminated from the background noise, while contributing only scarcely to the average intensity of the imaged area. In essence, the intrinsic noise originating *e.g.* from the detector, from the substrate's auto-fluorescence or from the presence of fluorescent molecules in solution is automatically suppressed from the evaluation. Also, variations in label brightness (*e.g.* associated with the distribution in size of the extruded vesicles) do not influence the signal, making quantitative estimates more accurate.

While background noise can be efficiently suppressed, a critical factor influencing the LOD of a bioanalytical assay exhibiting single-molecule sensitivity, such as the one reported here, is the background signal generated by non-specific binding events. Thus, an important aspect to be taken into consideration is the non-fouling character of the sensing interface which should, in this case, be virus but also vesicle repellent. The GSL-modified POPC supported lipid bilayers used in this work fulfilled these conditions, and the number of vesicles found on the negative controls varied between ~3 vesicles/frame (88 vesicles/mm^2) and ~ 35 vesicles/frame (1027 vesicles/mm^2), also if the bilayers were kept at room temperature overnight. Note in particular that 35 vesicles/frame corresponds to a coverage as low as 10^{-7}% of full coverage.

In spite of the good non-fouling properties of the surface coating, we demonstrate that equilibrium fluctuation analysis has the potential of further pushing down the background signal of the biosensor and of increasing the s/b: we take advantage of the partially reversible character of the vesicle-VLP interaction to discriminate specific from non-specific events based on their affinity to the sensing interface. Although demonstrated at the specific example of a sensor for the detection of the norovirus using receptor-containing lipid vesicles with a curvature

that reduces the affinity [32], the approach is in principle generic and applicable to both weak and strong binders. It can be applied to any biomolecular interaction provided that, for the experimental setup under consideration, the specific and non-specific interactions have a distinct characteristic kinetic behavior allowing for the determination of an optimal residence time window in which the equilibrium fluctuation analysis measurement should be performed. Besides the fact that the background signal can, in principle, be pressed down to zero as achieved for our platform, a major advantage of such an approach over conventional end-point measurements is that the performance of the biosensor is likely to be less dependent on the quality of the sensor's chemical interface. This in turn reduces the need for high-performance protein repellent coatings, which have so far played a crucial role in the performance of sensors with single-molecule sensitivity. Moreover, the availability of high affinity binders might become less critical and effort can be put on utilizing weak but highly specific binders which were so far discarded from affinity-based biosensor applications.

Conclusions

To conclude, we have demonstrated that a relatively simple assay setup combined with single-molecule sensitivity and equilibrium fluctuation analysis can be used to detect viral particles with a LOD in the low fM regime (i.e. $\sim 10^6$ particles/ml). The LOD was therefore in the same range, if not slightly better than what has so far been reported by others, also in the context of biosensors for the detection of noroviruses [8,9]. Without the need of any particle enrichment steps, these sensitivities are already sufficient to detect viral particles recovered from feces [8]. However, to meet the challenge of detecting norovirus particles in contaminated water, the focus of future development needs to be put on implementing particle enrichment steps to concentrate samples containing as little as 0.5–4 particles/ml [45]. Furthermore, to test the applicability of our platform for real diagnostic applications, efforts will now need to be directed at testing the sensor with biologically relevant samples which include stool, food and water sample as well as swabs from surfaces in restaurants and hospitals. Another aspect to be taken into consideration is the specificity of the assay. Histo-blood group antigens on glycosphingolipids, such as H type 1 have been shown to bind to noroviruses with high specificity although it cannot be excluded that they react with other species, in particular rotaviruses [46]. If needed, the specificity of the assay could be further optimized by using a combination of two different ligands in the sandwich assay format. In particular the glycolipids on the bilayer or on the vesicle could be replaced by an antibody against the virus which can provide additional genotype specificity. Such antibodies are commonly used in ELISA-based assays for NoV detection, but not in formats offering single virus sensitivity [8]. Additionally, real-time monitoring of binding reactions on a single particle level allows, in principle, for discrimination between different viral species according to their kinetic signatures. This aspect could further contribute to increase the assays specificity and will be the subject of further investigation.

Although optimization of the assay time was beyond the scope of this project, the whole assay could be performed within less than 2 hours. Currently, the major limiting factor towards shorter analysis time is the VLP incubation step (1 hour); read-out can be performed within minutes. A natural extension of the assay would be to skip the initial incubation step, and instead record transient binding events from a suspension containing a mixture of viruses and vesicles. This strategy would in fact work excellently for most sandwich assays, since the surface-bound probe and the secondary binder are typically directed to different (and single) epitopes on the target molecule. However, a virus typically contains a large number of identical epitopes, which means that the addition of vesicles can lead to aggregation. In this particular case, it is more relevant to stress that thanks to the simplicity of the fluorescence-based transduction, our assay is directly compatible with microfluidic devices that could, for example, integrate a sample pre-concentration step [9] or for optimized flow-based capture efficiency [47]. This could potentially increase the LOD by at least one order of magnitude. If assay time is not critical, the diffusion limitations inherent to assays performed under stagnant conditions could also be overcome by increasing the assay time (*e.g.* to overnight incubation) in order to maximize the VLP capture efficiency at the sensing interface without sacrificing the compatibility of our assay with the conventional microtiter plates format. Finally, each vesicle, containing around 3% fluorescent lipids is easily detectable at an acquisition time of 100 ms. Although a relatively advanced imaging set up (a 60× oil immersion TIRF objective and a cooled CCD camera) was employed, this points towards the opportunity to significantly simplify the detection system without scarifying the single-molecule sensitivity.

Additional file

Additional file 1: Figure S1. Dissociation behavior of the negative controls for bilayers of different quality. **Figure S2**. Response curve displayed vs. time evaluated using a residence time interval $\Delta\tau > 10$ s.

Competing interests

The authors declare that they have no competing interests.

Authors' contributions

The project was formulated by FH and MB. MB wrote the manuscript. MG performed the experiments. FP provided the virus-like particles. Manuscript completion was performed by all authors. All authors read and approved the final manuscript.

Acknowledgements
The work was supported by grants from Vinnova, the Swedish Research Council (8266 to GL), and t1he Swiss National Science Foundation (MB).

Author details
[1]Department of Applied Physics, Division of Biological Physics, Chalmers University of Technology, Göteborg SE-412 96, Sweden. [2]Instituto Universitario de Biotecnología de Asturias, Departamento de Bioquímica y Biología Molecular Universidad de Oviedo, Oviedo, Spain. [3]Department of Clinical Chemistry and Transfusion Medicine, Sahlgrenska Academy, University of Gothenburg, Gothenburg, Sweden.

Received: 23 October 2012 Accepted: 19 December 2012
Published: 6 February 2013

References

1. Chandra H, Reddy PJ, Srivastava S (2011) Protein microarrays and novel detection platforms. Expert Rev Proteomics 8(1):61–79
2. Templin MF, et al. (2002) Protein microarray technology. Trends Biotechnol 20(4):160–166
3. Teste B, Descroix S (2012) Colloidal nanomaterial-based immunoassay. Nanomedicine 7(6):917–929
4. Bally M, et al. (2006) Optical microarray biosensing techniques. Surf Interface Anal 38(11):1442–1458
5. Nagl S, Schaeferling M, Wolfbeis OS (2005) Fluorescence analysis in microarray technology. Microchimica Acta 151(1–2):1–21
6. Storhoff JJ, et al. (2005) *Labels and Detection methods* in *Microarray Technology and its Applications*. Springer, Berlin
7. Bally M, Voros J (2009) Nanoscale labels: nanoparticles and liposomes in the development of high-performance biosensors. Nanomedicine 4(4):447–467
8. Rabenau HF, et al. (2003) Laboratory diagnosis of norovirus: Which method is the best? Intervirology 46(4):232–238
9. Connelly JT, et al. (2012) Micro-total analysis system for virus detection: microfluidic pre-concentration coupled to liposome-based detection. Anal Bioanal Chem 402(1):315–323
10. Liu WT, et al. (2005) Microfluidic device as a new platform for immunofluorescent detection of viruses. Lab Chip 5(11):1327–1330
11. Donaldson KA, Kramer MF, Lim DV (2004) A rapid detection method for Vaccinia virus, the surrogate for smallpox virus. Biosens Bioelectron 20 (2):322–327
12. Ossiboff RJ, Parker JSL (2007) Identification of regions and residues in feline junctional adhesion molecule required for feline calicivirus binding and infection. J Virol 81(24):13608–13621
13. Drygin YF, et al. (2012) Highly sensitive field test lateral flow immunodiagnostics of PVX infection. Appl Microbiol Biotechnol 93(1):179–189
14. Driskell JD, et al. (2005) Low-level detection of viral pathogens by a surface-enhanced Raman scattering based immunoassay. Anal Chem 77(19):6147–6154
15. Su LC, et al. (2012) Rapid and Highly Sensitive Method for Influenza A (H1N1) Virus Detection. Anal Chem 84(9):3914–3920
16. Ilic B, Yang Y, Craighead HG (2004) Virus detection using nanoelectromechanical devices. Appl Phys Lett 85(13):2604–2606
17. Perez JM, et al. (2003) Viral-induced self-assembly of magnetic nanoparticles allows the detection of viral particles in biological media. J Am Chem Soc 125(34):10192–10193
18. Patolsky F, et al. (2004) Electrical detection of single viruses. Proc Natl Acad Sci USA 101(39):14017–14022
19. Hassen WM, et al. (2011) Quantitation of influenza A virus in the presence of extraneous protein using electrochemical impedance spectroscopy. Electrochim Acta 56(24):8325–8328
20. Valanne A, et al. (2005) A sensitive adenovirus immunoassay as a model for using nanoparticle label technology in virus diagnostics. J Clin Virol 33(3):217–223
21. Bally M, Dhumpa R, Voros J (2009) Particle flow assays for fluorescent protein microarray applications. Biosens Bioelectron 24(5):1195–1200
22. Bally M, et al. (2011) Fluorescent vesicles for signal amplification in reverse phase protein microarray assays. Anal Biochem 416(2):145–151
23. Bally M, et al. (2010) Liposome and Lipid Bilayer Arrays Towards Biosensing Applications. Small 6(22):2481–2497
24. Reichert J, et al. (2000) Chip-based optical detection of DNA hybridization by means of nanobead labeling. Anal Chem 72(24):6025–6029
25. Oldenburg SJ, et al. (2002) Base pair mismatch recognition using plasmon resonant particle labels. Anal Biochem 309(1):109–116
26. Gunnarsson A, et al. (2008) Single-molecule detection and mismatch discrimination of unlabeled DNA targets. Nano Lett 8(1):183–188
27. Laue M, Bannert N (2010) Detection limit of negative staining electron microscopy for the diagnosis of bioterrorism-related micro-organisms. J Appl Microbiol 109(4):1159–1168
28. Glasmastar K, et al. (2002) Protein adsorption on supported phospholipid bilayers. J Colloid Interface Sci 246(1):40–47
29. Chan YHM, Boxer SG (2007) Model membrane systems and their applications. Curr Opin Chem Biol 11(6):581–587
30. Christensen SM, Stamou DG (2010) Sensing-Applications of Surface-Based Single Vesicle Arrays. Sensors 10(12):11352–11368
31. Bally M, et al. (2012) Interaction of virions with membrane glycolipids. Phys Biol 9(2):026011
32. Bally M, et al. (2011) Interaction of Single Viruslike Particles with Vesicles Containing Glycosphingolipids. Phys Rev Lett 107(18):181103
33. Gunnarsson A, et al. (2011) Kinetics of Ligand Binding to Membrane Receptors from Equilibrium Fluctuation Analysis of Single Binding Events. J Am Chem Soc 133(38):14852–14855
34. Gunnarsson A, et al. (2009) Kinetic and thermodynamic characterization of single-mismatch discrimination using single-molecule imaging. Nucleic Acids Res 37(19):e99
35. Prasad BVV, et al. (1999) X-ray crystallographic structure of the Norwalk virus capsid. Science 286(5438):287–290
36. Mattison K (2011) Norovirus as a foodborne disease hazard. Adv Food Nutr Res 62:1–39
37. Kitamoto N, et al. (2002) Cross-reactivity among several recombinant calicivirus virus-like particles (VLPs) with monoclonal antibodies obtained from mice immunized orally with one type of VLP. J Clin Microbiol 40 (7):2459–2465
38. Rydell GE, et al. (2011) Susceptibility to winter vomiting disease: a sweet matter. Rev Med Virol 21(6):370–382
39. Rydell GE, et al. (2009) QCM-D studies of human norovirus VLPs binding to glycosphingolipids in supported lipid bilayers reveal strain-specific characteristics. Glycobiology 19(11):1176–1184
40. Karlsson KA, Larson G (1981) Molecular Characterization of Cell-Surface Antigens of Fetal Tissue - Detailed Analysis of Glycosphingolipids of Meconium of a Human-O Le(a-B+) Secretor. J Biol Chem 256(7):3512–3524
41. Nilsson J, et al. (2009) Norwalk virus-like particles bind specifically to A, H and difucosylated Lewis but not to B histo-blood group active glycosphingolipids. Glycoconj J 26(9):1171–1180
42. Boga JA, et al. (2004) Etiology of sporadic cases of pediatric acute gastroenteritis in Asturias, Spain, and genotyping and characterization of norovirus strains involved. J Clin Microbiol 42(6):2668–2674
43. Fiege B, et al. (2012) Molecular Details of the Recognition of Blood Group Antigens by a Human Norovirus as Determined by STD NMR Spectroscopy. Angew Chem Int Ed 51(4):928–932
44. Keller CA, Kasemo B (1998) Surface specific kinetics of lipid vesicle adsorption measured with a quartz crystal microbalance. Biophys J 75(3):1397–1402
45. Yang N, et al. (2012) Prevalence and diversity of norovirus genogroups I and II in Hong Kong marine waters and detection by real-time PCR. Mar Pollut Bull 64(1):164–168
46. Hu LY, et al. (2012) Cell attachment protein VP8*of a human rotavirus specifically interacts with A-type histo-blood group antigen. Nature 485(7397):256–259
47. Schoch RB, Cheow LF, Han J (2007) Electrical detection of fast reaction kinetics in nanochannels with an induced flow. Nano Lett 7(12):3895–3900

doi:10.1186/1559-4106-8-4
Cite this article as: Bally *et al.*: **A virus biosensor with single virus-particle sensitivity based on fluorescent vesicle labels and equilibrium fluctuation analysis.** *Biointerphases* 2013 **8**:4.